IEEE Access
Multidisciplinary ⋮ Rapid Review ⋮ Open Access Journal

Received October 20, 2020, accepted November 11, 2020, date of publication November 24, 2020,
date of current version December 7, 2020.

Digital Object Identifier 10.1109/ACCESS.2020.3040035

Direct Drop-on-Demand Printing of Molten Solder Bumps on ENIG Finishing at Ambient Conditions Through StarJet Technology

ZHE SHU[1], MICHAEL FECHTIG[1], FLORIAN LOMBECK[2], MATTHIAS BREITWIESER[1,2], ROLAND ZENGERLE[1,2], AND PETER KOLTAY[1,2]

[1]Laboratory for MEMS Applications, IMTEK-Department of Microsystems Engineering, University of Freiburg, D-79110 Freiburg, Germany
[2]Hahn-Schickard-Gesellschaft für angewandte Forschung e.V., D-79110 Freiburg, Germany

Corresponding author: Zhe Shu (zhe.shu@imtek.uni-freiburg.de)

This work was supported by the Federal Ministry of Education and Research (Germany) under Grant BMBF, FKZ 01QE1704C / E! 10998 P3D, Grant FKZ 02P16K014, and Grant FKZ 16ES0943.

ABSTRACT In this paper, we report on a detailed experimental study carried out with the StarJet technology to investigate the mechanical adhesion properties of directly printed solder bumps on electroless nickel immersion gold (ENIG) plated PCB boards. The aim of this study is to determine the maximum bond strength achievable by this method and to find suitable printing parameters that allow for the production of reliable and consistent solder bumps by non-contact printing of molten solder (type SAC305). Molten solder droplets of about 250 μm diameter were printed at melt temperatures between 250 and 400 °C onto ENIG surfaces kept at temperatures in the range of 100 to 200 °C. Using shear force tests, the adhesion of the printed bumps was investigated as a function of the main process parameters: 1. printhead temperature, 2. substrate temperature, and 3. substrate preheating time. The formation of an intermetallic compound (IMC) between the solder and the ENIG was confirmed by scanning electron microscopy (SEM) and energy-dispersive X-ray spectroscopy (EDX) measurements. As a result of the comprehensive experimental parameter study, suitable printing parameters for establishing bond strengths corresponding to maximum shear force values of 3000 to 4000 mN could be found, i.e. high printhead temperature of 400 °C, short preheating and time of < 2 min, and substrate heating at 180 °C The use of flux was found to slightly improve the bond strength and to improve the consistency of the printing results for extended operation times. The achieved high bond strength and the reasonable reproducibility of the printing results qualify the StarJet technology for further investigations regarding applications in the field of direct soldering of microelectronic chips and devices to PCB boards as well as other micro-assembly tasks in the future.

INDEX TERMS StarJet technology, soldering, metal droplets, drop-on-demand, metal printing, ball grid array, non-contact printing, bonding, intermetallic compound, experimental parameter study, suitable printing parameter, soldering materials.

I. INTRODUCTION

The prosperous microelectronics industry is one of the foundations of the great developments in the 20th century. In addition to the technologies related to integrated semiconductor devices, electronic packaging and assembly technologies are also important key technologies supporting the microelectronics industry. In the current decade, the highly miniaturized and multifunctional microelectronics, embedded electronics, microelectromechanical systems (MEMS) and internet of things (IoT) devices are demanding increasingly cost-efficient, miniaturized, and digital manufacturing. Further industrial requirements for packaging and assembly technologies are a high degree of automation and integration, high production speed, and compatibility with other technologies such as flexible electronics and organic semiconductor technologies [1], [2].

The traditional process for electrically contacting microelectronic chips requires various steps and processes that might evoke temperature or mechanical stress during the

The associate editor coordinating the review of this manuscript and approving it for publication was Jenny Mahoney.

fabrication. This can lead to process designs that are incompatible with alternative polymer technologies and do not fit well with the requirements of flexible digital fabrication. Consequently, some novel packaging technologies for directly soldering and interconnecting electronic components and printed circuit boards (PCBs) in two (2D) and three (3D) dimensions have been developed. The so-called contact-free metal deposition techniques, such as laser solder jetting [3]–[5], inkjet printing of solder droplets [6], [7], and Ag nanoparticle-based inks [8]–[10], can deposit conductive metal without directly contacting the sample and provide various advantages such as high compatibility with 3D structures and flexible PCBs, low local heating while establishing the electrical contact, avoiding direct contamination and damage, and reduced process steps and cost due to the digital fabrication concept.

Amongst all these contact-free metal deposition methods, the StarJet direct printing technology provides a single-step, non-contact metallization by directly applying molten metal droplets in liquid state for metallization and soldering on various materials in 2D and 3D. The technology is based on a pneumatically driven printhead including a heatable reservoir for the molten metal and an interchangeable nozzle chip featuring a star-shaped orifice geometry. Detailed information about the working principle and the specifications of the StarJet technology can be found in our previous publications [11]–[13]. Different printhead prototypes based on the StarJet method can be operated at temperatures above melting temperatures of metals such as solder [12] and aluminum alloys [14]. Compared to the aforementioned metallization technologies, the StarJet technology provides additional advantages due to the direct interconnection and bonding by the molten solder applied in liquid state. By rapid solidification of the solder, also printing of 2D and 3D metal structures is possible in addition to the electrical connection established by the solder. By working with molten solder material, the troublesome laser safety issues and costly setup of other beam-based and solder ball technologies can be avoided. Thanks to the local inert atmosphere provided by the nitrogen rinse gas, StarJet printheads can directly operate at ambient conditions and eliminate the high cost of maintaining an inert atmosphere such as a glovebox. The rinse gas also supports the precise droplet deposition from a large distance of several millimeters up to two centimeters to control thermal impact on 3D structures as well as on polymer substrates, while still providing high printing precision.

Although the StarJet technology has been successfully applied to electrical interconnections on PCBs [15] and flexible polymer foils [16], metallization for solar cells [17], and 3D metallic structures [11], [18], there is still no systematic analysis of the interaction of molten solder droplets on commonly used electronic contact pads having an ENIG (electroless nickel immersion gold) finishing. Therefore, this paper is intended to provide a first comprehensive study of the adhesion properties of solder bumps printed via the contact-free drop-on-demand StarJet technology on ENIG surfaces, commonly used in microelectronics for PCB and chip metallization. The SAC305 (Sn96.5Ag3Cu0.5) has been used in the investigation as it is the industrial standard and widely used in microelectronic assembly and packaging. The quantitative assessment of the achievable electrical conductivity and mechanical stability of the solder bumps at different process parameters can pave the way for industrial applications of direct soldering to produce reliable electrical interconnections in microelectronics, by this low-cost, non-contact, digital printing method.

II. EXPERIMENTAL

A. MATERIAL

The bare printed circuit boards (PCB) with ENIG finishing were provided by PragoBoard s.r.o., Czech Republic. The ENIG coating consists of a nickel layer with a thickness of $\sim$3 μm and a gold layer with a thickness of $\sim$100 nm. Underneath there is a copper layer with a thickness of $\sim$35 μm. The bulk solder used for this research is lead-free solder SAC305 (Sn96.5Ag3Cu0.5). The non-clean flux paste (MG chemical 8341) was purchased from RS Components GmbH, Germany and used directly without any further modification.

B. EXPERIMENTAL SETUP

To perform the investigation, a StarJet printhead is mounted onto a Spectrum II dispensing system by Nordson Asymtek, USA (see Fig. 1). It features a programmable, three-axis motion system with a positioning precision of $\pm$15 μm. A top-view camera setup allows alignment and inline position control. The StarJet printhead was connected to the existing pneumatic dispensing system. The print height was controlled by the Nordson Asymtek Spectrum II z-axis control. A tactile height sensor calibrates the printing height before every printing sequence. The customized substrate holder includes a resistive heater, which can heat the whole substrate area up to 300 °C. The resistive heater is the heating block under the substrate and powered by a thyristor (Schneider Electric Eurotherm 7100A) and regulated with a thermocouple sensor and a PID control unit. Nitrogen was used as actuation gas as well as rinse gas to actuate the ejecting and to protect the jetted molten solder from oxidization, respectively. The diameters of printed molten metal droplets can be adjusted by changing the StarJet nozzle chip featuring a star-shaped orifice geometry. The orifice of the nozzle chip is kept at 183 μm throughout the whole experiment.

C. STABILITY OF DROPLET GENERATION

Before the experiment, a large quantity of solder droplets was printed and characterized to ensure reproducible results. A self-developed stroboscopic setup was used to evaluate the droplet formation and stability. In order to check the jetting stability of the StarJet technology, various printhead temperatures ($T_{printhead}$) have been selected in the range from 250 to 415 °C to characterize the droplet size and consistency. As can be seen from **TABLE 1**, a large number of droplets

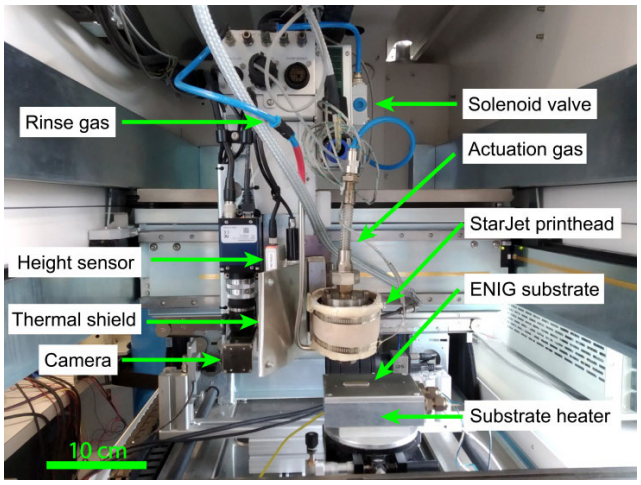

FIGURE 1. StarJet printing system. The StarJet printhead is mounted on the Nordson Asymtek Spectrum II dispensing platform with a customized substrate holder. There are two independent gas supplies. A constant rinse gas pressure establishes a flow through star-shaped bypass channels and provides an inert gas shielding of the printed molten metal. The actuation gas pressure is used to apply pressure to the reservoir via a solenoid valve to trigger the ejection of droplets or jets.

TABLE 1. List of parameters and results of stability test of droplet jetting via StarJet drop-on-demand mode by a stroboscopic characterization setup.

$T_{printhead}$ [°C]	# of tested droplets	Average droplet diameter [µm]	Standard deviation of droplet diameter [µm]	CV
250	5072	245	1.3	0.55%
270	13300	255	1.9	0.75%
300	10037	249	1.4	0.56%
320	11759	252	2.4	0.94%
335	5343	251	3.2	1.28%
385	5435	254	1.2	0.46%
415	2011	253	1.2	0.47%

has been tested, and stable single droplets with an average diameter of 245 to 255 μm with very low coefficient of variation (CV) $< 1.3\%$ could be produced at all tested temperatures. This provides a solid foundation for the parameter study on the interaction of jetted molten solder droplets on ENIG surfaces on PCB boards. Consequently, it is justified to assume that all the solder droplets, printed at various printing conditions, have approximately the same droplet diameter.

D. EXPERIMENTAL PROCEDURE

For the static thermal impact investigation in Section III.A, samples were printed at substrate temperature (T_{sub}) of 20 °C (room temperature), 50, 100, 120, 150, 180, and 200 °C. The printhead temperature was fixed at 250, 320, and 400 °C, which are 33, 103, and 183 °C above the melting point of SAC305 solder (217 °C). In total, 50 droplets were printed for each temperature set. The sample was placed on the substrate heater when the temperature T_{sub} had been reached and stabilized. To allow for a homogeneous heating, the sample settled on the heater for at least 60 s before the start of the printing.

For the dynamic thermal impact investigation in Section III.B, the substrate holder was first heated to the target temperature (e.g. 120 °C). After the target temperature was reached and stabilized, a PCB sample was placed on the substrate holder. The first array with 4 × 4 droplets was then printed 35 s after the initial placement. The droplets were placed, in x and y direction, with a 1.3 mm pitch to the center of the next droplet. The second array was then printed on the same substrate 120 s after the initial placement. Further arrays were printed on the same substrate at 300 and 480 s after the initial placement. In total, for each substrate and printhead temperature, one ENIG sample with four arrays of 16 droplets were printed.

E. CHARACTERIZATION METHODS

The electrical conductivity between the ENIG and the solder bumps was generally so high that the contact resistance could not be measured with a conventional multimeter. Therefore, the electrical contact resistance of the bumps can be considered as sufficiently low for microelectronic applications and was not characterized any further.

To characterize the adhesion between printed the solder bumps and the ENIG surface, a shear-off test was performed using a Nordson DAGE 4000 bondtester machine. A photograph of the setup and an illustration of the measurement are depicted in the supporting material, Figure S1. A ball shear test routine with a BS5kg tool cartridge was utilized. To perform the test, the machine places a chisel tool in a shear off height of 55 μm with respect to the detected substrate surface. During the measurement, the sample is moved in an orthogonal path toward the chisel with a speed of 250 μm/s while the shear force experienced by the tool is measured.

To observe the oxidation and intermetallic compound (IMC) growth, also cross-sections of selected solder bumps were prepared. The samples were overcast with a high-viscosity cyanoacrylate-based resin (VariDur 10, Bühler Group). During hardening at air, a cyanoacrylate matrix forms, which serves as the mechanical support for the grinding process. The rough grind was performed with a silicon carbide polishing wheel. In a next step, the cut was polished with a diamond polishing slurry (MAGNUM-TOP-DUO, Microdiamant). In a last step, a diamond suspension up to 1/4 μm was used for fine finishing. Scanning electron microscope (SEM) images were recorded on an Amber X microscope from the company Tescan with an accelerating voltage of 20 kV and a beam current of 100 pA. The signal was detected with an Everhart–Thornley detector. Energy dispersive X-ray (EDX) spectra/images were captured using an Octane Elite Plus detector from the company EDAX. Excitation voltage was set at 20 kV, and beam currents of 30 pA, 100 pA, 300 pA, and 1 nA were used and compared to ensure absence of artifacts.

F. FAILURE MODE DURING SHEAR FORCE TEST

During the experimental shear force tests, two different failure modes have been observed: ball lift-off and ball

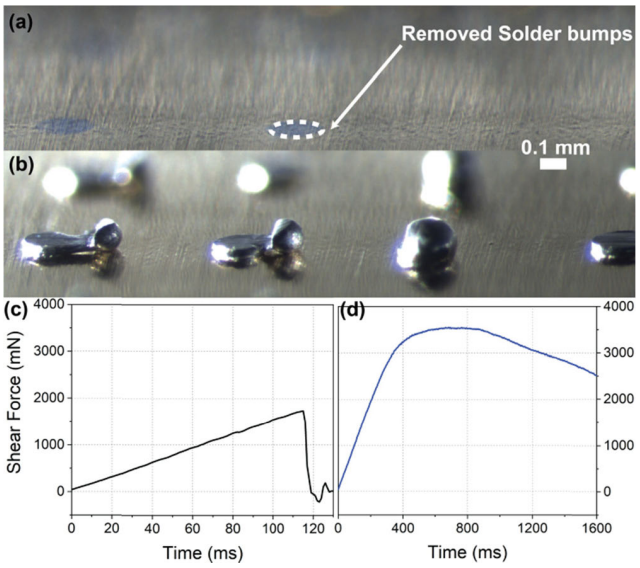

FIGURE 2. Failure modes during shear-off testing. (a) Printed solder bumps lifted off completely, (b) and printed solder bumps deformed by the shear tool. (c) Typical shear force test diagram where a lift-off occurs during the measurement (cf. image (a)). (d) Typical shear force test where the bump is totally deformed (cf. image (b)).

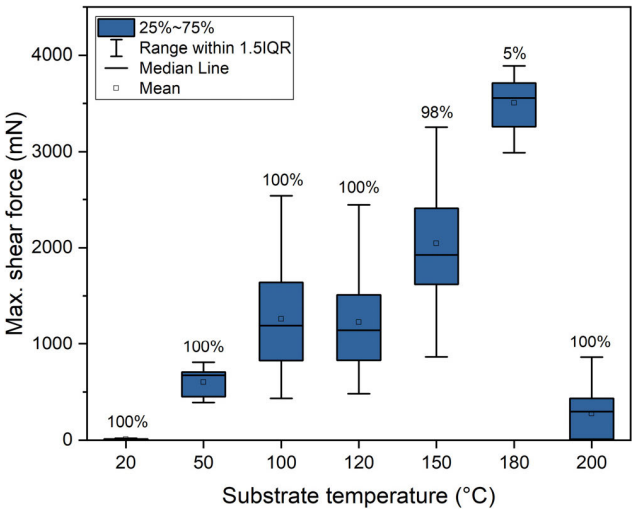

FIGURE 3. Maximum shear forces of printed solder bumps printed on PCB samples with ENIG finishing as a function of substrate temperature during printing. The numbers on top of the box diagram show the percentage of bumps that where sheared off (see Fig. 2a,c) at the specific parameter settings. The printhead temperature has been kept at 320 °C throughout the experiments. For the droplet group printed with T_{sub} = 20 °C (room temperature), the shear force was below the measurement limit of the measurement setup.

deformation, as can be seen from the Fig. 2a,b. In some cases, the printed solder bumps are lifted off the substrate by the shear force measurement tool when the formed IMC is not strong enough. In other cases, when the IMC creates a bond that is stronger than the material, the solder bumps are deformed and their base remains attached to the PCB at the original position. The typical threshold where the lift-off failure mode changes into the deformation failure mode is at a shear force value of about ∼3000 mN with some variation. The exact value highly depends on the contact area between measurement tool and the printed solder bumps as well as the contact area between the printed solder bumps on the ENIG surface. Typical shear force measurements resulting from the two different failure modes — ball lift-off mode and ball deformation mode — are shown in Fig. 2c,d.

III. RESULTS AND DISCUSSION

Thermal energy level and thermal gradients play important roles in the metallurgical reactions of molten solder on ENIG surfaces. During a traditional soldering process on ENIG finishing, the gold layer rapidly dissolves into the liquid solder [19]. Due to the thin gold layer thickness, only a negligible amount of Sn-Au compound is created [20]. Nevertheless, the thin gold layer is needed to prevent oxidation of the nickel layer. After the dissolution of the gold layer, the molten solder contacts the nickel layer directly, and the tin and nickel atoms diffuse into each other as they have high kinetic energy due to substrate heating and high thermal energy of the solder bumps. Consequently, the nickel and tin form a Ni-Sn compound during solidification. Below 260 °C, mainly Ni_3Sn_4 is formed. While Ni_3Sn_2 and Ni_3Sn compounds form at temperatures between 240 and 300 °C, crystalline structures are built up at 400 °C [21]. These metallurgical reactions form the physical connection between the metal pad and the solder, depending on the effective temperature level and duration of heating. To form strong mechanical connections, it is important that the thickness of the IMC layer is balanced. No IMC layer at all indicates no mechanical connection, while an IMC layer with excessive thickness, on the other hand, can lead to defects and weaker connections, due to the brittle nature of the IMC [21]–[23].

The non-contact soldering on ENIG surfaces via direct metal printing as provided by the StarJet technology has a fundamentally different thermal interaction as well as dynamics compared to the industrial reflow process. Due to the tiny amount of jetted solder with limited thermal energy, the maximum attainable temperature level, as well as the duration of the heat pulse, is very small. This particularly occurs when the PCB samples are not heated up above the melting temperature of the solder (i.e. 217 °C) to prevent the ENIG surface from oxidation. Oxidation might happen when the printing process is performed under ambient conditions, and therefore the nickel atoms can diffuse through the ultra-thin gold layer (100 nm) and form oxides on top of the gold layer.

Due to the low thermal energy provided by the solder droplet, the solidification speed of the molten solder on the ENIG surface is very fast and there is only a limited time available for the reaction between tin and nickel to form the IMC. Therefore, the thermal balance between substrate temperature, printhead temperature and ambient temperature influences the mechanical stability of directly printed solder bumps, significantly. In the following, several temperature-related process parameters have been carefully examined to understand their impact.

A. STATIC THERMAL IMPACT

The adhesion of printed solder droplets on PCBs with ENIG finishing was first evaluated at various substrate temperatures (T_{sub}) ranging from 20 to 200 °C. The printhead temperature has been kept at 320 °C throughout these experiments. The experimental procedure to determine the adhesion by shear force measurements was described in Section II.E. The maximum shear strength over different substrate temperatures was also calculated and analyzed based on the measured data. The details can be found in the supporting material online. A detailed analysis reveals that the maximum shear strength shows the same trend for the overall adhesion as the maximum shear force, and therefore we decide to use only the maximum shear force as the measure throughout this paper. In Fig. 3, the maximum shear force values that occurred during a set of measurements are shown as box plots. Obviously, the maximum shear force and thus the adhesion increases with substrate temperature, before it drops to a very low value gain at 200 °C. In most experiments, the droplets were sheared off from the substrate at shear force values below 3000 mN. However, at 180 °C substrate temperature, where maximum shear force values of 3000 mN could be obtained, most of the droplets were not sheared off the substrate but were deformed without losing adhesion (see Fig. 2b,d). The percentage of printed bumps that were sheared off from the substrate is given for each experimental condition as a percentage on top of the box plot in Fig. 3 and also in all following figures.

As depicted in Fig. 3, the maximum shear force of samples printed at $T_{sub} < 120$ °C is close to the lower threshold of the measurement setup. More specifically, at $T_{sub} = 50$ °C, only 7 out of 20 measured droplets exceed this threshold. At $T_{sub} = 20$ °C, no droplet exceeded the threshold. This clearly indicates that the thermal energy of the molten solder droplet is not high enough to dissolve the gold layer and to form an IMC. The increasing adhesion from 120 to 180 °C can be explained by the increasing solidification time of the solder ball on the substrate. This increases the time for the diffusion-driven IMC formation. The deeper diffusion leads to the formation of a thicker IMC layer before the droplet solidifies. Up to a certain degree, a higher IMC thickness leads to a higher adhesion. If the IMC exceeds a certain thickness, the inhomogeneous inner crystal needle structure of Ni-Sn IMC leads to an overall more brittle structure. This brittle structure shows a lack of mechanical stability and leads to failure[21], [24], [25]. However, besides the diffusion of solder into the nickel layer, it must be considered that the substrate heating can also lead to a diffusion of nickel through the gold layer of the ENIG coating [20]. It has also been found out that the annealing of ENIG surfaces at elevated temperature at 150 °C for as short as 5 min will produce the excessive nickel oxides due to nickel atom diffusion [26]. Therefore, the higher substrate heating (e.g. 200 °C) also promotes the atom diffusion of the nickel through the gold layer and forms nickel oxidation, which reduces the surface wetting (contact area of the solder) and leads to smaller area

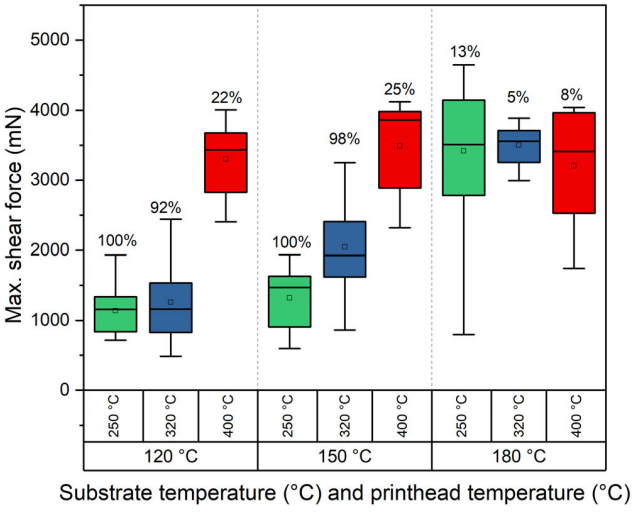

FIGURE 4. Maximum shear forces of printed solder bumps on PCB samples with ENIG finishing for printhead temperatures of 250, 320, and 400 °C as a function of the substrate temperature during printing. The numbers on top of the box diagram show the percentage of bumps that were sheared off the substrate.

for forming IMC layers [27] The contact area between printed solder bumps and the ENIG surface reduces significantly from 180 to 200 °C substrate temperature (see Figure S1, column 2 and 3 in the supporting document). The reduction in maximum shear-off force at 200 °C could therefore be explained by a combination effect of nickel oxide layer and too thick and brittle IMC due to a higher substrate temperature.

In order to further investigate these failure mechanisms, one can increase the local thermal energy for solder diffusion and keep the diffusion rate of the nickel atoms in the ENIG surface constant. Thus, the balance between the two described effects can be shifted. In the present case, this can be achieved by varying the temperature of the molten solder while keeping the substrate temperature constant. Fig. 4 depicts the adhesion variation of printed solder bumps on ENIG surfaces — again in terms of maximum shear force and displayed as box plots like in Fig. 3 — at three different printhead temperatures of 250, 320, and 400 °C for three different substrate temperatures of 120, 150, and 180 °C. The data clearly show that the adhesion of printed solder bumps on the ENIG surface increases with higher printhead temperature, i.e. higher thermal energy of the molten solder droplets for all substrate temperatures. For the lowest substrate temperature, the highest relative increase of the adhesion can be found. This clearly indicates that at lower substrate temperatures, the adhesion is limited by the diffusion of the tin and therefore the IMC cannot be fully developed, which leads to a reduced mechanical stability of the printed solder bumps. It is interesting to see that there is an upper adhesion limit at substrate temperature of 180 °C. At this temperature, the temperature of the impinging droplets does not seem to matter, and all experiments show comparable and high maximum shear force values, as well as a very low fraction of bumps that

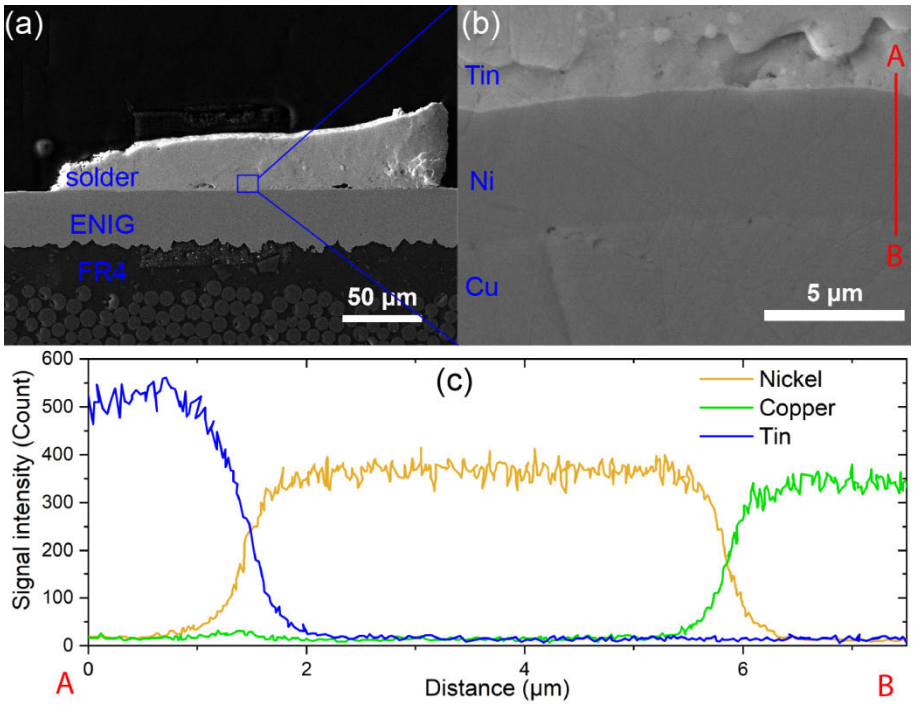

FIGURE 5. SEM micrographs of a printed solder bump on ENIG finishing. The solder bump was printed at $T_{printhead} = 400$ °C and $T_{sub} = 150$ °C without flux layer. Three different images of the same sample are shown in (a) and (b) at increasing magnification. Clearly, a thin IMC layer can be observed between the nickel layer and the SAC solder layer in (b). (c) A line measurement by EDX was taken along the line indicated by a red bar in (b) from position A to B. The corresponding material distribution is shown along the line: blue = tin, yellow = nickel, green = copper.

could be sheared off the substrate, which is smaller than for any other substrate temperature.

To clearly see the interface and the IMC interlayer, the printed sample with printhead temperature of 400 °C and substrate temperature of 150 °C has been imaged by SEM and EDX. The imaged solder bump was first measured via the shear force measurement setup and deformed during this measurement, but it did not shear off the substrate. A cross-section was prepared from this sample like described in Section II.E. From the SEM image shown in Fig. 5, it can be seen that there is a thin interlayer with a layer thickness of approximately 1 μm between the printed solder and nickel layer. The interlayer thickness of the interface between tin and nickel is roughly calculated as, as seen in Fig. 5c, the overlapping length where the signal of tin declines from the average maximum to the average minimum and the rising signal of nickel from average minimum to average maximum. From the EDX measurement, a smooth transition from tin to nickel and nickel to tin is present at this position (see Fig. 5c). A similar transition is also present at the nickel and copper interface. This suggests that there could be a tin-nickel alloy formed at the interface between the printed solder bump and the ENIG surface.

B. DYNAMIC THERMAL IMPACT

To further investigate the impact of the substrate heating, particularly its duration, on the adhesion properties of the bumps, a time-dependent experiment has been conducted to study the relationship between adhesion and oxidation of the surface. Due to nickel atoms diffusing through the gold at elevated temperatures, an oxide might be formed at the surface. In the following experiment, the ENIG samples were preheated for various time duration, i.e. 35, 120, 300, and 480 s, before deposition of molten solder droplets. As observed in the previous experiments, the largest change can be expected at substrate temperatures of 120, 150, and 180 °C. Thus, these three substrate temperatures have been selected for this evaluation. The experimental procedure is described in Section II.D in detail. The measured maximum shear force of printed solder bumps on ENIG samples at $T_{sub} = 120$, 150, and 180 °C as a function of preheating time is plotted in Fig. 6. For each parameter combination, 16 printed solder bumps have been measured by the shear force tests.

It can be clearly seen in Fig. 6 that the adhesion of printed solder bumps on the ENIG surface decreases as the preheating time increases. While for 120 °C this effect is hardly significant, the adhesion is reduced at higher substrate temperatures down to about 30% of the value obtained without preheating. This result shows that the transient dynamics of the ENIG surface temperature plays a crucial role for the non-contact soldering process. This result suggests that over time an oxidation of the ENIG finishing might take place at substrate temperatures above 120 °C that impedes the IMC layer formation required for high adhesion.

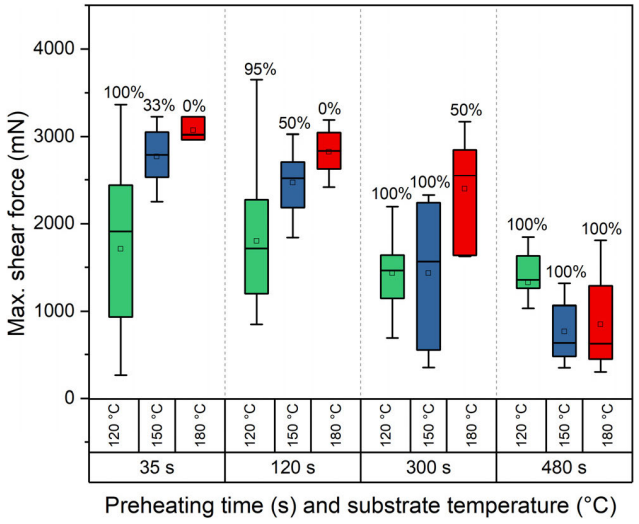

FIGURE 6. The maximum shear forces of printed solder bumps on PCB samples with ENIG finishing, printed after preheating times of 35, 120, 300 and 480 seconds and at various substrate temperatures of 120, 150, and 180 °C. The printhead temperature has been kept at 320 °C throughout the experiment. The numbers on top of the box diagram show the percentage of bumps that were sheared off the substrate.

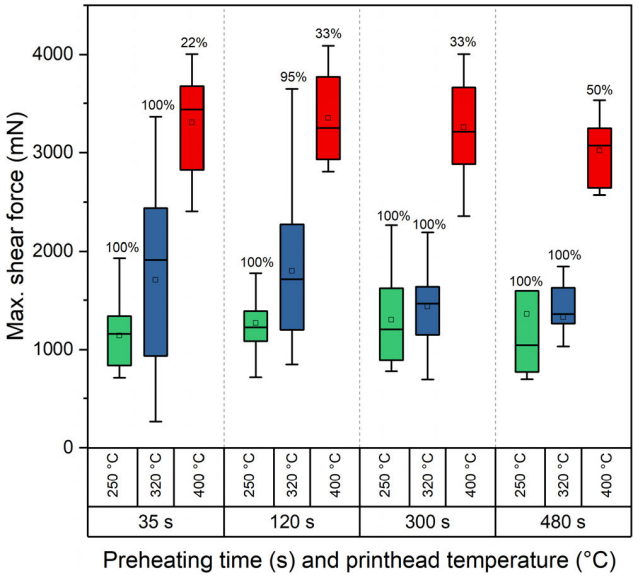

FIGURE 7. Maximum shear forces of printed solder bumps on PCB samples with ENIG finishing, printed after preheating times of 35, 120, 300, and 480 seconds and at various printhead temperatures of 250, 320, and 400 °C. The substrate temperature has been kept at 120 °C throughout the experiment. The numbers on top of the box diagram show the percentage of bumps that were sheared off the substrate.

Similar investigations of the influence of the preheating duration were carried out at different printhead temperatures. The results of the corresponding shear-off test are plotted in Fig. 7. The substrate temperature of 120 °C was selected because the preheating duration showed little influence on the adhesion in the previous experiments at this value. Similar conclusions as for the static investigation with different printhead temperatures can also be drawn in this case: Higher thermal energy of molten solder leads to higher adhesion. Furthermore, for all tested temperatures the adhesion did not decrease significantly with increasing preheating time of the substrate. Therefore, a substrate temperature not higher than 120 °C and a printhead temperature of 400 °C seem to be suited for practical applications, where the substrate is exposed to the elevated temperature for a longer time. First, this is because the duration of preheating does not play a significant role for the adhesion, and thus the loading of PCBs and any interruptions during the printing process are not critical. Second, this is because high maximum shear forces can be still achieved that are in the order of magnitude of the mechanical properties of the bulk solder. Nevertheless, at this condition still about 22 to 50% of the bumps are sheared off the substrate at maximum shear force of about 3000 mN. In order to obtain low or zero shear-off failures, short preheating times and substrate temperature of about 180 °C, as shown in Fig. 6, might be more preferable.

C. IMPACT OF FLUX

Although flux-free processes are highly preferred in industrial production, it is still interesting to know to what extent flux can influence the adhesion. Therefore, similar experiments have been performed as the previous ones with variable substrate temperature and preheating time.

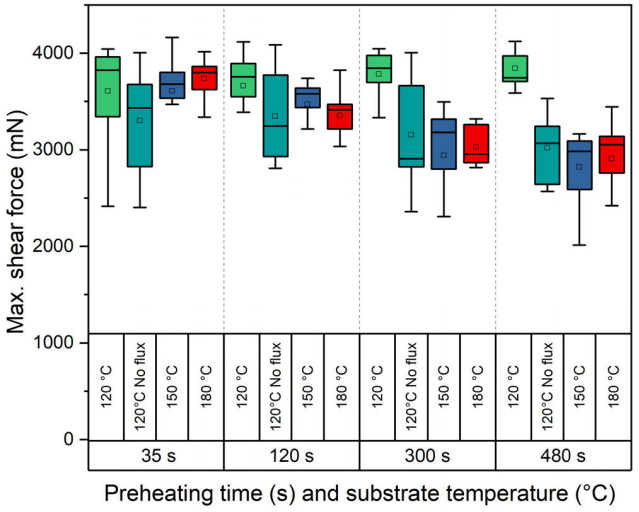

FIGURE 8. Maximum shear forces of printed solder bumps on PCB sample with ENIG finishing with flux coating, which were printed after preheating times of 35, 120, 300, and 480 seconds and at various substrate temperatures of 120, 150, and 180 °C. The printhead temperature has been kept at 400 °C throughout the experiment.

The procedure is described in Section II.D in detail. The printhead temperature was fixed at 400 °C as it provided the best performance in the previous experiments. The maximum shear force measurement results for fluxed samples printed at different substrate temperatures are plotted in Fig. 8. The results obtained without flux at $T_{sub} = 120$ °C are also added to the diagram for comparison. The diagram indicates that the additional non-clean flux further improves the adhesion and largely reduces the preheating-induced adhesion issue discussed before. Regardless of the preheating time, high

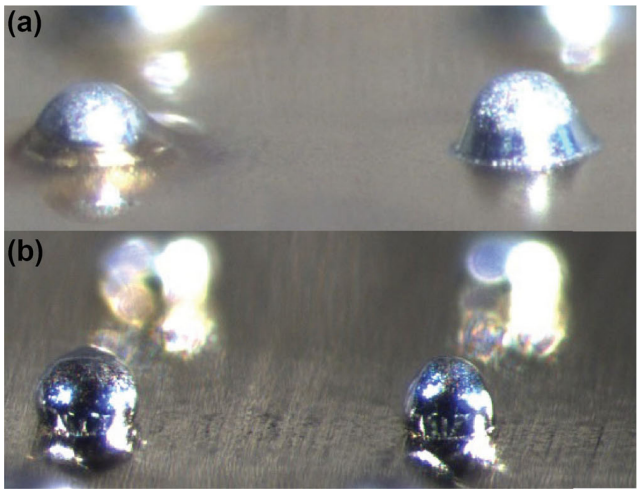

FIGURE 9. Side view photograph of printed solder bumps on PCB samples with ENIG finishing: (a) with a non-clean flux layer; and (b) without flux layer. They were both printed at printhead temperature of 400 °C and substrate temperature of 180 °C.

shear-off values can be obtained that are limited by material properties of the tin only and not by the adhesion to the substrate. The reason for this is probably because the additional flux layer prevents nickel from direct contact with oxygen, even when it has diffused to the surface due to extended preheating. If we compare the adhesion properties of printed solder bumps with and without flux layer at $T_{sub} = 120$ °C, there is generally a slight increase of the maximum shear forces. This increase might be explained by the different contact area of printed bumps with and without flux due to the additional wetting property of the flux that leads to a more stable bump geometry and a higher contact area (see Fig. 9).

Finally, it is also interesting to note that the use of flux reduces the variability of the adhesion for nearly all tested conditions. Compared to the results without flux (see Fig. 6), the distribution of the data is narrower for nearly all tested conditions. Narrow distributions without flux were rarely obtained in most of the other reported experiments.

IV. CONCLUSION

In this experimental study, we have shown that molten solder droplets printed by StarJet technology can be used to produce solder bumps with low electrical resistance and high mechanical adhesion on ENIG surfaces. Therefore, the StarJet technology has high potential in direct soldering, bumping and electrical bonding of microelectronic devices and chips on PCBs. The main process parameters affecting the adhesion between solder and ENIG have been studied in detail, and it turned out that the printhead temperature, the substrate temperature, as well as the preheating time of the substrate are crucial parameters that influence the formation of the IMC by which the mechanical adhesion and electrical conductivity are mediated.

In order to achieve bonding strengths suitable for industrial applications, corresponding to values of 3000 mN maximum shear force or higher, the molten solder (type SAC305) should be applied at high temperatures in the range of 300 to 400 °C on ENIG surfaces heated to about 180 °C. Under these conditions, a quite narrow distribution of high maximum shear-off forces can be obtained. The interface of the printed solder bumps on the ENIG surface was also examined via SEM and EDX. A thin interlayer can be observed, which could be the IMC layer for high adhesion. If the substrate has to be kept at high temperature for a longer time (e.g. due to extended printing duration for a whole PCB board), then reducing the substrate temperature down to 120 °C can be beneficial. This is because diffusion of nickel can take place through the thin gold layer at elevated temperatures over time and then lead to reduced adhesion of the solder. In our experiments, heating times of more than 120 s at temperatures above 150 °C were sufficient to observe a reduction of adhesion.

Finally, it could be shown that the use of flux (MG chemical 8341 flux paste) can further improve the maximum shear force to above 4000 mN by providing a larger contact area for the bumps and a lower bump profile. Furthermore, flux reduces the negative impact of extended substrate heating times and generally improves the consistency between individual bumps. Therefore, the additional effort of applying flux can be rewarded by an easier adjustment of appropriate printing parameters as well as a more robust and consistent performance over time.

ACKNOWLEDGMENT

The authors thank M. Feißt (IMTEK, Freiburg, Germany) for preparing the metallographic grinds. The article processing charge was funded by the Baden-Wuerttemberg Ministry of Science, Research and Art and the University of Freiburg in the funding programme Open Access Publishing.

REFERENCES

[1] H. Lim, H. S. Kim, R. Qazi, Y. Kwon, J. Jeong, and W. Yeo, "Advanced soft materials, sensor integrations, and applications of wearable flexible hybrid electronics in healthcare, energy, and environment," *Adv. Mater.*, vol. 32, no. 15, Jul. 2019, Art. no. 1901924, doi: 10.1002/adma.201901924.

[2] Y. Khan, A. Thielens, S. Muin, J. Ting, C. Baumbauer, and A. C. Arias, "A new frontier of printed electronics: Flexible hybrid electronics," *Adv. Mater.*, vol. 32, no. 15, Nov. 2019, Art. no. 1905279, doi: 10.1002/adma.201905279.

[3] M. Mäusezahl, M. Hornaff, T. Burkhardt, and E. Beckert, "Mechanical properties of laser-jetted SAC305 solder on coated optical surfaces," *Phys. Procedia*, vol. 83, pp. 532–539, Jan. 2016, doi: 10.1016/j.phpro.2016.08.055.

[4] W. Yue, M.-B. Zhou, and X.-P. Zhang, "Reliability and failure analysis of electronic components induced by the reflection of laser beam in the laser jet solder ball bonding process," in *Proc. 18th Int. Conf. Electron. Packag. Technol. (ICEPT)*, Aug. 2017, pp. 1658–1662, doi: 10.1109/ICEPT.2017.8046754.

[5] P. Ribes-Pleguezuelo, B. Septriani, S. Zhang, E. Beckert, R. Eberhardt, F. Wyrowski, and A. Tünnermann, "Solderjet bumping packaging technique optimization for the miniaturization of laser devices," *J. Eur. Opt. Soc.-Rapid Publications*, vol. 13, no. 1, p. 34, Dec. 2017, doi: 10.1186/s41476-017-0063-7.

[6] W. R. Cox, C. Guan, D. J. Hayes, and D. B. Wallace, "Microjet printing of micro-optical interconnects," *Int. J. Microcircuits Electron. Packag.*, vol. 23, no. 3, pp. 346–352, 2000.

[7] C.-H. Wang, W.-S. Hwang, W.-M. Chen, H.-L. Tsai, and C.-H. Wu, "Molten lead-free solder deposited by inkjet printing for bonding of thin-film solar cell modules," *Mater. Trans.*, vol. 57, no. 6, pp. 797–804, 2016, doi: 10.2320/matertrans.MD201501.

[8] E. Sowade, M. Polomoshnov, A. Willert, and R. R. Baumann, "Toward 3D-printed electronics: Inkjet-printed vertical metal wire interconnects and screen-printed batteries," *Adv. Eng. Mater.*, vol. 21, no. 10, Oct. 2019, Art. no. 1900568, doi: 10.1002/adem.201900568.

[9] J. A. Sadie and V. Subramanian, "Three-dimensional inkjet-printed interconnects using functional metallic nanoparticle inks," *Adv. Funct. Mater.*, vol. 24, no. 43, pp. 6834–6842, Nov. 2014, doi: 10.1002/adfm.201401312.

[10] B. Khorramdel, T. M. Kraft, and M. Mäntysalo, "Inkjet printed metallic micropillars for bare die flip-chip bonding," *Flexible Printed Electron.*, vol. 2, no. 4, Dec. 2017, Art. no. 045005, doi: 10.1088/2058-8585/aa9171.

[11] N. Lass, B. Gerdes, M. Jehle, L. Riegger, R. Zengerle, and P. Koltay, "Generation of high aspect ratio metal microstructures exhibiting low surface roughness by drop-wise printing of liquid metal," *Procedia Eng.*, vol. 120, pp. 1103–1106, Jan. 2015, doi: 10.1016/j.proeng.2015.08.791.

[12] N. Lass, L. Riegger, R. Zengerle, and P. Koltay, "Enhanced liquid metal micro droplet generation by pneumatic actuation based on the StarJet method," *Micromachines*, vol. 4, no. 1, pp. 49–66, Mar. 2013, doi: 10.3390/mi4010049.

[13] N. Lass, "Pneumatically actuated high temperature resistant printhead for molten metals based on the StarJet principle," Ph.D. dissertation, Dept. Eng., Albert-Ludwigs-Universität Freiburg, Freiburg im Breisgau, Germany, 2016.

[14] B. Gerdes, M. Jehle, M. Domke, R. Zengerle, P. Koltay, and L. Riegger, "Drop-on-demand generation of aluminum alloy microdroplets at 950 °C using the StarJet technology," in *Proc. 19th Int. Conf. Solid-State Sensors, Actuat. Microsyst. (TRANSDUCERS)*, Jun. 2017, pp. 690–693, doi: 10.1109/TRANSDUCERS.2017.7994142.

[15] M. Jehle, B. Gerdes, P. Soukup, M. Fechtig, R. Zengerle, Koltay, and L. Riegger, "Direct printing of electrical connections from metal melts using StarJet technology," in *Proc. IEEE 19th Electron. Packag. Technol. Conf. (EPTC)*, Dec. 2017, pp. 1–4, doi: 10.1109/EPTC.2017.8277490.

[16] Z. Shu, B. Gerdes, M. Fechtig, L. Riegger, R. Zengerle, and P. Koltay, "Direct printing of conductive metal lines from molten solder jets via StarJet technology on thin, flexible polymer substrates," in *Proc. NIP Digit. Fabr. Conf.*, vol. 2018, no. 1, Sep. 2018, pp. 72–75, doi: 10.2352/ISSN.2169-4451.2018.34.72.

[17] B. Gerdes, M. Jehle, N. Lass, L. Riegger, A. Spribille, M. Linse, F. Clement, R. Zengerle, and P. Koltay, "Front side metallization of silicon solar cells by direct printing of molten metal," *Sol. Energy Mater. Sol. Cells*, vol. 180, pp. 83–90, Jun. 2018, doi: 10.1016/j.solmat.2018.02.022.

[18] B. Gerdes, R. Zengerle, P. Koltay, and L. Riegger, "Direct printing of miniscule aluminum alloy droplets and 3D structures by StarJet technology," *J. Micromech. Microeng.*, vol. 28, no. 7, Jul. 2018, Art. no. 074003, doi: 10.1088/1361-6439/aab928.

[19] F.-Q. Li and C.-Q. Wang, "Influence of interfacial reaction between molten SnAgCu solder droplet and Au/Ni/Cu pad on IMC evolution," *Trans. Nonferrous Met. Soc. China*, vol. 16, no. 1, pp. 18–22, Feb. 2006, doi: 10.1016/S1003-6326(06)60004-6.

[20] R. B. Cinque and J. W. Morris, "The effect of gold-nickel metallization microstructure on fluxless soldering," *J. Electron. Mater.*, vol. 23, no. 6, pp. 533–539, Jun. 1994, doi: 10.1007/BF02670656.

[21] T. Laurila, V. Vuorinen, and J. K. Kivilahti, "Interfacial reactions between lead-free solders and common base materials," *Mater. Sci. Eng., R, Rep.*, vol. 49, nos. 1–2, pp. 1–60, Mar. 2005, doi: 10.1016/j.mser.2005.03.001.

[22] J. C. Madeni, S. X. Liu, and T. A. Siewert, "Intermetallics formation and growth at the interface of tin-based solder alloys and copper substrates," in *Proc. 2nd Int. Brazing Soldering Conf.*, 2003, pp. 1–9.

[23] L. Xu and J. H. L. Pang, "Intermetallic growth studies on SAC/ENIG and SAC/CU-OSP lead-free solder joints," in *Proc. Thermal Thermomech. 10th Intersociety Conf. Phenomena Electron. Syst., ITHERM*, May 2006, pp. 1131–1136, doi: 10.1109/ITHERM.2006.1645472.

[24] N. Jiang, L. Zhang, Z.-Q. Liu, L. Sun, W.-M. Long, P. He, M.-Y. Xiong, and M. Zhao, "Reliability issues of lead-free solder joints in electronic devices," *Sci. Technol. Adv. Mater.*, vol. 20, no. 1, pp. 876–901, Dec. 2019, doi: 10.1080/14686996.2019.1640072.

[25] A. Choubey, H. Yu, M. Osterman, M. Pecht, F. Yun, L. Yonghong, and X. Ming, "Intermetallics characterization of lead-free solder joints under isothermal aging," *J. Electron. Mater.*, vol. 37, no. 8, pp. 1130–1138, Aug. 2008, doi: 10.1007/s11664-008-0466-8.

[26] C. C. Lee, H. Y. Chuang, C. K. Chung, and C. R. Kao, "Oxidation behavior of ENIG and ENEPIG surface finish," in *Proc. 5th Int. Microsyst. Packag. Assem. Circuits Technol. Conf.*, Oct. 2010, pp. 1–4, doi: 10.1109/IMPACT.2010.5699652.

[27] D. Goyal, T. Lane, P. Kinzie, C. Panichas, K. M. Chong, and O. Villalobos, "Failure mechanism of brittle solder joint fracture in the presence of electroless nickel immersion gold (ENIG) interface," in *Proc. 52nd Electron. Compon. Technol. Conf.*, May 2002, pp. 732–739, doi: 10.1109/ECTC.2002.1008179.